ACS OMEGA

http://pubs.acs.org/journal/acsodf
Article

Mechanism and Performance Evaluation of a Strain Sensor Made from a Composite Hydrogel Containing Conductive Fibers of Thermoplastic Polyurethane and Polyvinyl Alcohol

Ming Kong, Ruiyu Zhou, Min Yang,* Jun Zhang, Xiao Ma, Teng Gao, Yanbin Zhang, Benkai Li, Mingzheng Liu, Xin Cui, Yunze Long, and Changhe Li

Cite This: *ACS Omega* 2024, 9, 43743−43755

ABSTRACT: Monitoring human physiological conditions using flexible, stretchable strain sensors is an effective approach to prevent and treat critical illnesses, emergencies, and infectious diseases. However, achieving ultralow detection limits, high sensitivity, and a wide detection range in a cost-effective manner is challenging. In this study, a strain sensor was developed by embedding an adhesive hydrogel composed of polyvinyl alcohol, starch, and glutaraldehyde into conductive fibers made from thermoplastic polyurethane. By leveraging the high sensitivity of the conductive fibers and the wide detection range of the hydrogel, a robust dual-layer continuous conductive network was formed through their synergistic interaction. Tensile strength tests and other assessments indicated that the sensitivity of the sensor increased from a gauge factor of 49.32 (for fiber-based sensors) to 74.18, while the detection range expanded from 250 to 400%. Furthermore, the sensor demonstrated a low detection limit (0.6%), fast response and recovery times (80 ms/120 ms), and durability exceeding 800 cycles. Tests on pulse monitoring, joint movement, and voice recognition confirmed the significant applicability of the sensor for real-time monitoring of various physiological activities throughout a human's life. This study aims to provide technical support for the development of flexible wearable systems.

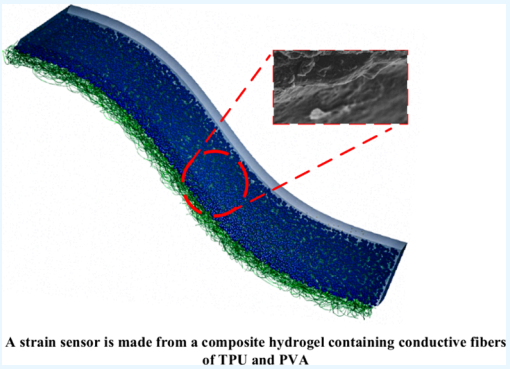

1. INTRODUCTION

Wearable strain sensors are integral components of flexible smart electronic devices. They play a crucial role in human motion and health monitoring, especially in situations where diseases such as cardiac conduction disorders and arrhythmias pose serious threats to physical and mental well-being during physical activity and rest.[1−5] Resistive strain sensors, which are characterized by their low cost, simple processing and design, and high signal readability, are promising types for applications in real-time intelligent healthcare and medical care systems.[6−12] However, wearable resistive strain sensors still encounter challenges related to achieving a broad detection range, high sensitivity, rapid response, and low detection limits. Therefore, a rational structural design and excellent material selection are necessary strategies to address these issues.[13−19]

In recent years, many high-performance piezoresistive strain sensors have been constructed using biomimetic spider microcrack structures. This biomimetic spider microcrack structure, with its unique fracture and closure characteristics, can induce a significant change in resistance during the stretching process. Shen et al.[20] developed a piezoresistive strain sensor using a conductive polymer composite material, which is characterized by high sensitivity (strain coefficient, GF 602), a wide detection range (90%), low detection limit, and rapid response. Zheng et al.[21] utilized laser-induced graphene as the sensing layer, which employs a biomimetic spider web structure known with excellent resonance capability and robust performance. The sensor demonstrated high sensitivity (GF 36.8) with a detection range of 35%. Similarly, Wang et al.[22] designed a dual-layer conductive strain sensor with ultrahigh sensitivity (GF 1477.7) and a detection range of 150%, which meet the requirements for wearable sensors. However, this biomimetic spider microcrack structure, with its unique opening and closing sensing mechanism, undoubtedly imparts a limited sensing range. This limitation causes it to fail during intense large-strain body movements, which prevents the full utilization of the 600% stretchability of thermoplastic polyurethane (TPU) fibers.[23]

Received: July 8, 2024
Revised: September 22, 2024
Accepted: September 25, 2024
Published: October 16, 2024

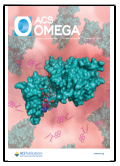

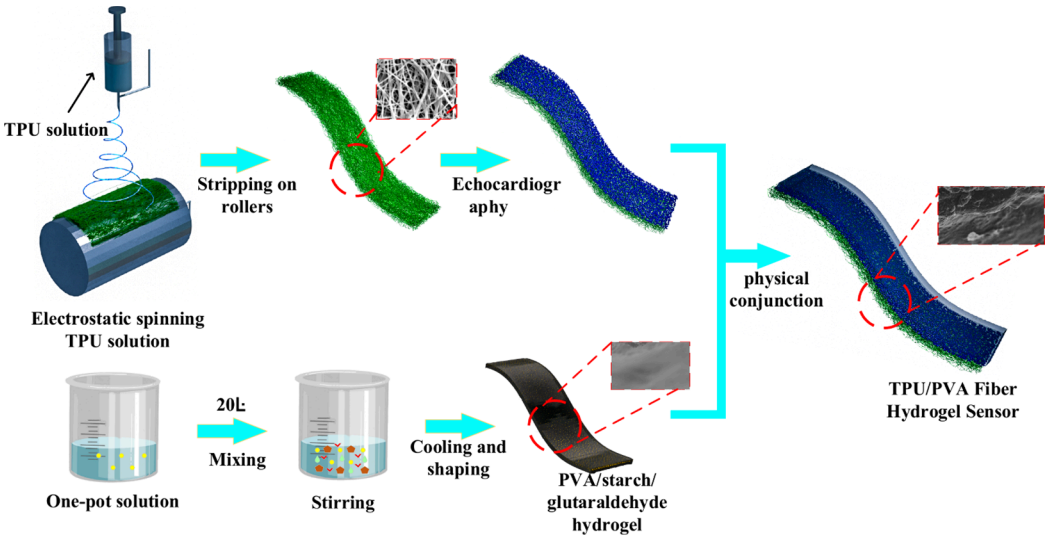

Figure 1. Fabrication of a flexible strain sensor through electrospinning and one-pot method.

The application of conductive hydrogels in flexible wearable devices has gained widespread attention. However, in the practical use of hydrogel sensors, realizing an extremely wide detection range but low sensitivity is challenging. For instance, Shen et al.[24] proposed a strain sensor made from a conductive polymer hydrogel with a detection range of 300%, low hysteresis, and a sensitivity of 4.07, which provides remote control signals for industrial robots. He et al.[25] utilized gelatin and PVA as the polymer framework, with tannin as the cross-linker, to prepare a gelatin composite hydrogel. The hydrogel exhibited excellent stretchability (760%) and a sensitivity of 6.79. Despite the critical drawback of low sensitivity, hydrogels possess outstanding advantages in self-repair and adhesion functionalities, which make them particularly advantageous in wearable devices. Xu et al.[26] developed a physically cross-linked ionogel with high conductivity (2.92 mS cm^{-1}) and excellent stretchability (2066%). Furthermore, the ionogel exhibited outstanding water resistance and underwater adhesion. The sensitivity of silicone gel strain sensors is low, and microcrack fiber sensors have a limited stretching range. Therefore, this study designs a dual-layer continuous conductive structure incorporating a strain sensor made from a composite hydrogel containing conductive fibers of TPU and PVA.

Flexible and stretchable strain sensors are crucial for monitoring human physiological conditions. However, a bottleneck issue exists due to the imbalance between sensitivity and detection range. Thus, this study designs a dual-layer continuous conductive structure incorporating a strain sensor made from a compositive hydrogel containing conductive fibers of TPU and PVA. The aim is to achieve a balanced trade-off between sensitivity and detection range by leveraging the respective advantages and disadvantages of biomimetic spider microcracks and hydrogels. The first layer of the structure consists of a TPU-supported Gr/CNT microcrack composite film, and the second layer is formed by combining PVA−starch as a polymer scaffold with conductive hydrogel. The first layer comprises a stretchable conductive network formed by varying the loading amount of Gr/CNT in the TPU fiber membrane. Subsequently, the prepared PVA−starch high-viscosity hydrogel forms another conductive structure under mechanical action, and the dual-layer continuous conductive network tightly integrates beneath the high viscosity of the hydrogel and the highly rough surface of the TPU fibers. The experimental results demonstrate that the performance of the strain sensor is excellent. It is designed to provide technical support for research on flexible wearable systems and comprehensive life-long physiological sign detection for individuals.

2. EXPERIMENTAL SECTION

The experimental section includes specific parameters for the preparation of a hydrogel composed of PVA, starch, and glutaraldehyde, details the process of fabricating TPU fiber membranes using electrospinning technology, and introduces the process parameters involved in electrospinning. It also explains the integration of Gr/CNT conductive load with the TPU fiber membrane. In the end, it describes the process of forming the flexible sensor, including the equipment used and the specific parameters involved in the characterization process.

2.1. Hydrogel Preparation. The preparation of hydrogels involves the combination of various functional materials. The one-pot preparation process, as illustrated in Figure 1, involves the mixing of 0.18 g borax and 4.5 mL ethylene glycol at 40 °C with stirring for 5 min. Subsequently, 15 mL deionized water and 0.3 g Gr/CNT are added, followed by ultrasonication at 40 °C for 30 min. Next, 12 g PVA, 12 g starch, and 1.4 g glutaraldehyde are added, and the mixture is stirred thoroughly at 100 °C for 5 h. Starch and PVA, which serve as the fundamental framework of the hydrogel, exhibit high stability. The introduction of borax forms dynamic cross-links through borate ester bonds, which enhance stability. The incorporation of Gr/CNT improves the electrical properties, while the addition of glutaraldehyde forms acetyl groups, which increases adhesion. Furthermore, the inclusion of EG enhances the moisturizing properties.

2.2. Preparation of TPU Nanofiber Membrane. First, the precursor solution is prepared by dissolving TPU particles in a mixture of DMF and THF (1:1) at 80 °C with stirring for 3 h, which results in a clear and uniform precursor solution with a concentration of 200 g/L. Subsequently, the solution is spun using a syringe with a 22-gauge needle at a spinning voltage of 14.5 kV, a spinning distance of 18 cm, a feed rate of

https://doi.org/10.1021/acsomega.4c06328
ACS Omega 2024, 9, 43743−43755

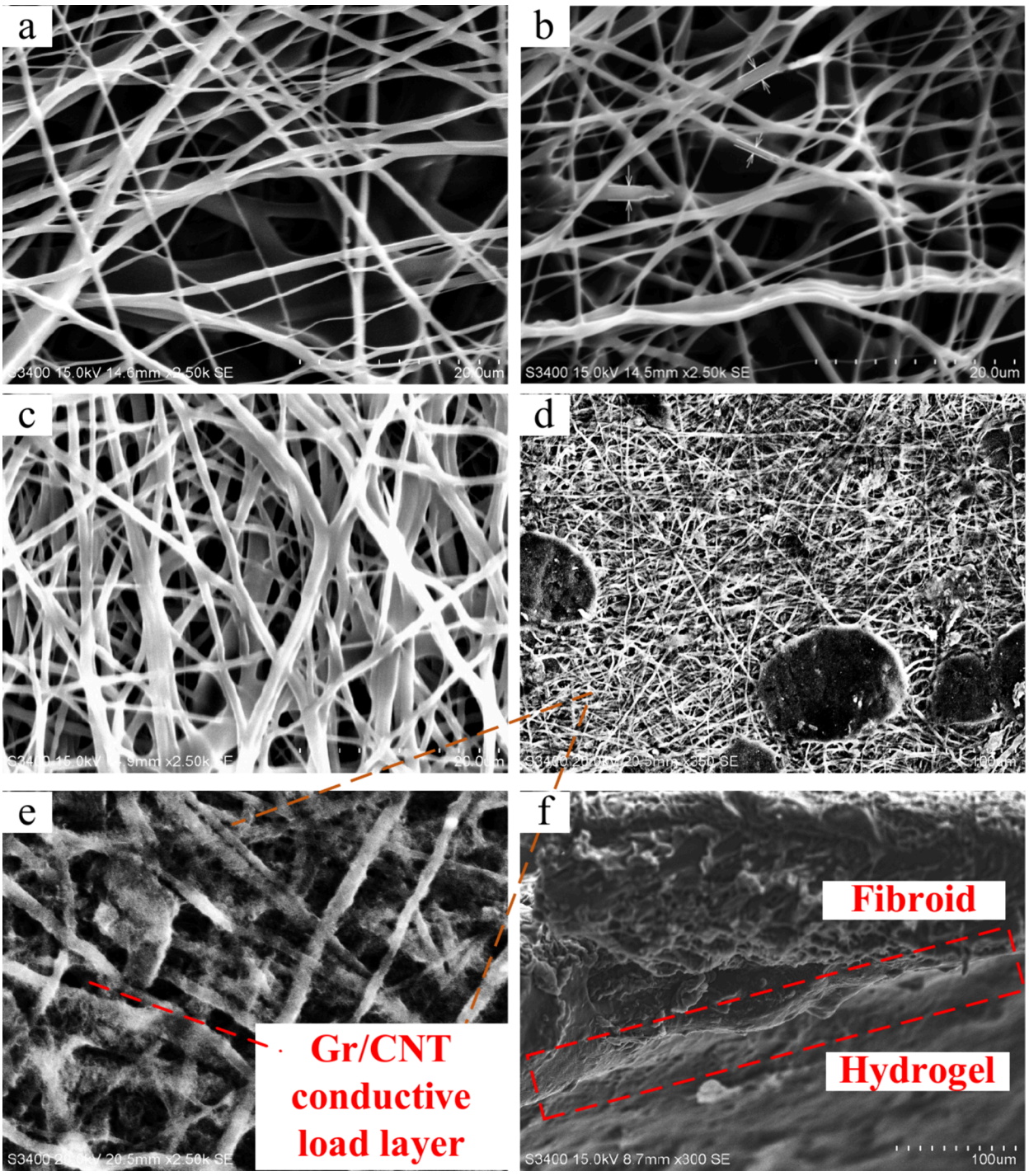

Figure 2. Characterization of TPU/Gr/CNT Fibers. (a, b) Untreated TPU fiber membrane. (c) SEM image of TPU fiber membrane after treatment. (d, e) SEM images of Gr/CNT/TPU fibers. (f) SEM image of the interface between fibers and hydrogel.

18 μL/min, and a drum speed of 325. Thus, the resulting nanofiber membrane is dried in a 70 °C oven for 2 h to remove residual solvent.

2.3. Preparation of Sensors. First, 40 mg of graphene and carbon nanotubes (in a 1:1 ratio) is dispersed in 20 mL of anhydrous ethanol, with sodium dodecyl sulfate added as a surfactant. The mixture is subjected to continuous ultrasonic vibration at 40 °C for 1 h to prepare a uniform suspension. The TPU nanofiber membrane is placed in a 2 g/L anhydrous ethanol solution and subjected to continuous ultrasonic vibration for 1 h. This process ensures the thorough deposition of nanoscale conductive materials onto the nanofiber membrane. The resultant is rinsed three times with distilled water, and then, it is dried in a 70 °C oven for 1 h. Next, the prepared hydrogel is fixed onto the nanofiber membrane with the deposited conductive material. Specifically, 0.1 g of the hydrogel is adhered onto a 3 × 2 nanofiber membrane.

2.4. Characterization and Testing. *2.4.1. Scanning Electron Microscope Testing.* The experimental process involves characterization of the fiber films composed of TPU and Gr/CNT using the Sigma300 scanning electron microscope (SEM) produced by Carl Zeiss, Germany. Initially, a

https://doi.org/10.1021/acsomega.4c06328
ACS Omega 2024, 9, 43743−43755

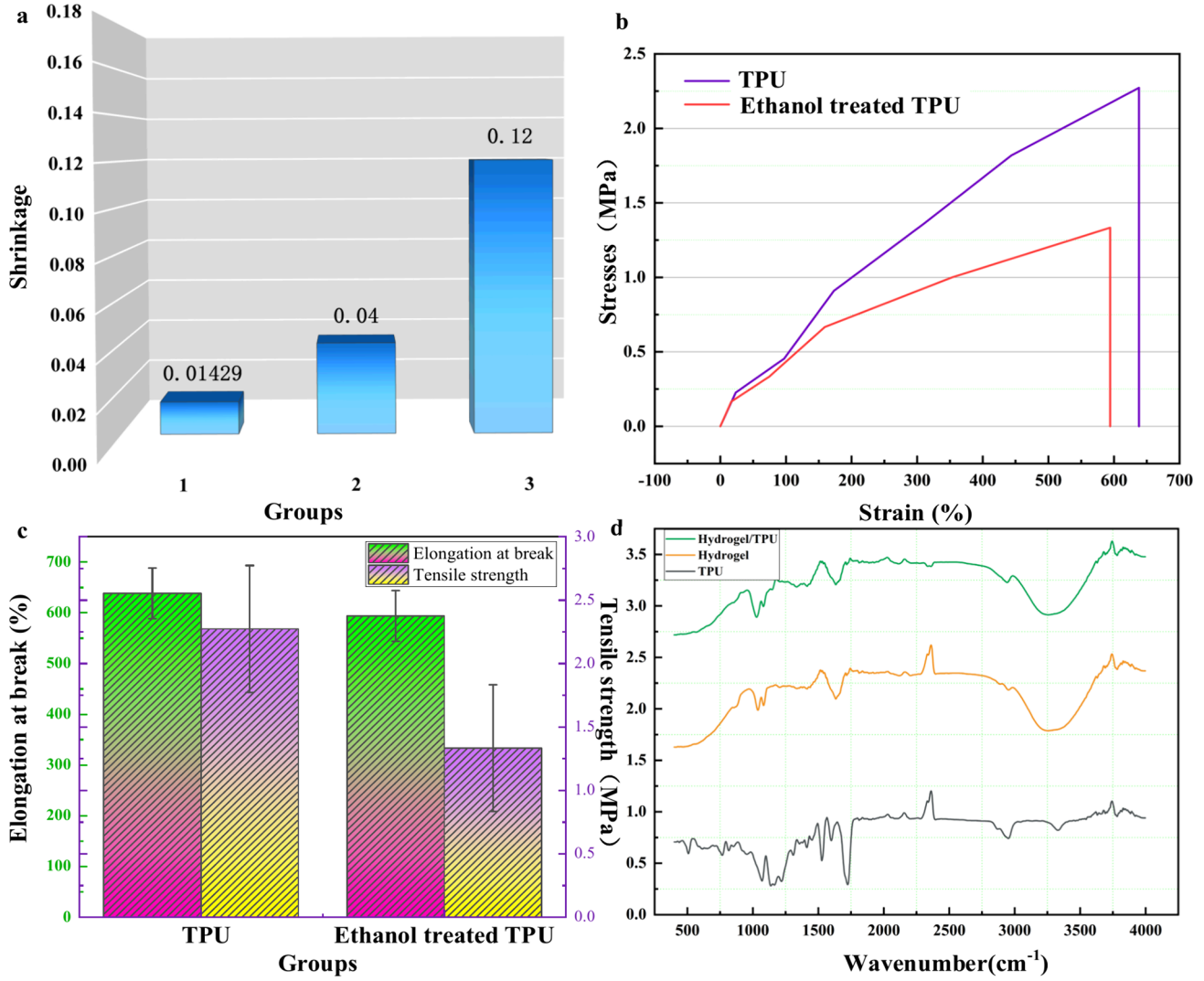

Figure 3. Tensile characterization of TPU fiber membrane. (a) TPU fiber shrinkage rate. (b) Stress−strain curves of TPU and TPU treated with ethanol. (c) Fracture elongation of TPU fibers. (d) FTIR images of fibers and their hydrogel.

gold sputter coating is applied to the fiber films. The fiber films are fixed onto metal discs using conductive adhesive in a longitudinal manner for ease of observation. Subsequently, they are sputter-coated with gold. The testing voltage is adjusted to 20 kV, as shown in Figure 3a.

2.4.2. X-ray Diffraction (XRD) and Fourier Transform Infrared Spectroscopy (FTIR). XRD analysis is performed using the Rigaku Miniflex 600 from Japan. X-ray diffraction patterns are used to analyze the distribution of atoms within different crystals. A copper target is utilized, and the scanning range is set to standard (10°−80°), specifically scanning angles are set from 10° to 80° at a speed of 10°/min.

Fourier transform infrared spectroscopy (FTIR) is conducted using the IS10 model from Thermo Fisher Scientific, USA, to characterize the main functional groups of the experimental samples.

2.4.3. Electromechanical Universal Testing Machine. The electronic universal testing machine used is the CMT6103 model manufactured by MTS (Mechanical Testing Systems). The testing is conducted at room temperature with a loading rate of 50 mm/min. Three repetitions are performed to obtain the average results of the tensile tests, which focus on stress−strain curves.

2.4.4. Sensitivity Detection Device. This study uses a self-prepared sensitivity detection device.

3. RESULTS AND DISCUSSION

In this section, several tests, from design and fabrication to characterization, are conducted on the sensor. The optimal structure and material combination are selected to identify the best-performing flexible sensor through testing.

3.1. Design of a Composite Hydrogel Containing Fibers of TPU and PVA. Based on the principle of resistive sensors, this study introduces a strain sensor utilizing a dual-layer continuous conductive structure integrating a composite hydrogel containing conductive fibers of TPU and PVA. The preparation of the flexible strain sensor with a dual-layer continuous conductive structure is illustrated in Figure 1. The upper layer of the structure consists of a conductive hydrogel made of PVA−starch, and the lower layer comprises conductive fibers. The continuous combination of the conductive fiber network and the PVA−starch hydrogel network enhances the effective stretchability of the conductive fibers while maintaining excellent electrical performance.

The synthetic method in this study involves the following steps. First, the lower substrate is prepared. The substrate is a

https://doi.org/10.1021/acsomega.4c06328
ACS Omega 2024, 9, 43743−43755

white TPU nanofiber membrane prepared by electrospinning. Subsequently, the nanofiber membrane is immersed in an ethanol solution of Gr/CNT. The Gr/CNT conductive load is modified onto the surface of the nanofiber membrane through thermal ultrasonic vibration. Consequently, the conductive nanofiber membrane exhibits a black color, which indicates the formation of the first layer of a conductive network. Simultaneously, a conductive gel with adhesiveness is prepared using a one-pot method. EG is dissolved in a solution with boric acid at 40 °C for 5 min. Thereafter, a mixture of Gr/CNT nanocomposite powder and deionized water is added, and the system is subjected to ultrasonic treatment for half an hour at 40 °C. Next, PVA, starch, and glutaraldehyde are added, and the mixture is thoroughly stirred at 100 °C for 5 h. Finally, the high-temperature gel is placed into a mold containing the conductive nanofiber membrane, pressurized, and cooled to room temperature. The multilayer cross-linking of the hydrogel facilitates the formation of the second layer of the conductive network structure. The high viscosity of the hydrogel made of PVA, starch, and glutaraldehyde allows achieving comprehensive integration of the fiber network and the hydrogel network using physical method alone.[27−35]

3.2. Fiber Morphology Structure and Characterization. Figure 2 illustrates the morphological characteristics of the fabricated network-like conductive structure for validating the effectiveness of constructing a dual-layer continuous conductive structure using fibers and hydrogel. The pure TPU fibers exhibit a smooth and uniform surface, with randomly oriented fibers and abundant internal voids (Figure 2a,b). The average diameter of the nanofiber membrane is approximately 1.1 μm. As depicted in Figure 2d,e, after ultrasonic treatment in a 2 g/L ethanol solution containing Gr/CNT, the surface roughness of the nanofibers significantly increases. By contrast, the ultrasonic treatment in ethanol solution alone, as shown in Figure 2c, does not cause any noticeable roughening of the fibers. This result indicates that the nanofibers are successfully coated with graphene and carbon nanotubes. The combination of the hydrogel and nanofibers is shown in Figure 2f. The interface clearly demonstrates the tight integration of the two materials, which forms a compact dual-layer continuous conductive structure.

This study observed that, at the macroscopic level, the TPU fiber membrane exhibits a noticeable contraction trend after ultrasonic ethanol treatment. Therefore, the tensile properties of TPU after contraction are investigated.[36,37] The nanofiber membrane is delaminated from the silicone paper on the drum and cut into rectangular samples with a length of 5 cm. The samples are then placed in 99% anhydrous ethanol and kept stationary for 1 h. As observed, the nanofiber membrane undergoes significant contraction. Figure 3a displays physical images before and after wetting with anhydrous ethanol, which reveal noticeable shrinkage of the nanofibers in different directions. The nanofiber is subjected to treatment at 50 °C−60 °C to validate the phenomenon of nanofiber contraction at high temperatures. The results showed that the shrinkage rate of the fiber membrane treated with anhydrous ethanol at room temperature is 1.429%, while the shrinkage rate of the nanofiber at high temperatures is 4%. This finding strongly confirms that high temperatures and 99% anhydrous ethanol contribute to the contraction of nanofibers.

The relationship between stress and strain for TPU nanofiber membranes is depicted in Figure 3b. As shown in the graph, the tensile strength of all samples falls between 1 and 3 MPa. In contrast to pure TPU nanofibers, TPU nanofibers treated with hot ethanol exhibit lower tensile strength. This reduction is accompanied by a simultaneous loss of fracture elongation, with fracture elongation rates ranging between 500% and 600%. The SEM images of the treated fibers are comprehensively investigated to determine the reasons for the loss of tensile performance. The fibers neither break nor exhibit significant internal damage under the effect of ultrasonic treatment. The simultaneous decrease in fracture elongation and tensile strength is attributed to the intrusion of high temperature and ethanol, which alters the atomic and molecular structure of TPU nanofibers. This alteration causes swelling within the fibers, which leads to a weakening of tensile performance. Alternatively, the decrease in tensile strength may be attributed to the release of fiber prestrain and the activation of responsive shape memory, which suggests a connection between the trend of fiber contraction and the fabrication process.[36] However, the Young's modulus of TPU nanofibers also decreases, which reduces from 3.55×10^{-3} to 2.23×10^{-3}. The reduction in the Young's modulus of flexible materials makes them softer, which improves the tactile feel for close contact. In addition, it enhances the flexibility, plasticity, and energy absorption properties. Thus, these materials are advantageous for applications such as wearable sensors where flexibility and sufficient toughness are key benefits.

Subsequently, the interface binding between TPU fibers and PVA hydrogel is investigated. The functional groups and interactions between the composite materials are characterized by FTIR, as shown in Figure 3d. The C−O−C stretching band of pure TPU nanofibers is represented by a characteristic peak at 1070 cm^{-1}, the N−H stretching vibration band is observed at 3328 cm^{-1}, and the absorption peaks at 2950 cm^{-1} correspond to the − CH stretching vibration. The absorption peaks at 1529 and 1725 cm^{-1} indicate the presence of the −H−N−COO− functional group. After the CNT/Gr loading treatment, the absorption peaks shift to 1594 and 1722 cm^{-1}. This shift is attributed to the hydrogen bonding between TPU and CNT. The characteristic peaks at 1070, 3328, and 2950 cm^{-1} have shifted to 1072, 3334, and 2952 cm^{-1}, respectively.[38−41]

In the infrared spectrum of the hydrogel, a stretching vibration peak of the O−H group is observed at 3239 cm^{-1}. This peak is attributed to the hydroxyl groups in the borate ester bonds and the molecular hydrogen bonds. The presence of absorption peaks at 1039 and 1083 cm^{-1} indicates stretching vibrations of B−O−C or C−O−C bonds, which suggests the formation of borate ester bonds in the hydrogel network. The presence of a peak at 1637 cm^{-1} corresponding to the C = O group indicates that hydroxyl groups (−OH) in some starch react with carbon aldehyde groups (C = O) in glutaraldehyde, which forms acetal linkages. The results confirm that the hydrogel is based on glutaraldehyde, with multiple cross-linking involving PVA, starch, ethylene glycol, and borax.[42,43] Finally, the FTIR spectrum of the hydrogel attached to the fibers represents a combination of the fiber and hydrogel spectra due to physical interactions. The degree of their binding is characterized, as shown in Figure 2f, which reveals a seamless integration. Despite hydrogel rupture during the tensile experiment, no delamination occurs between the hydrogel and fibers, which indicates a strong bond.

3.3. Strain Sensing Performance. The design of a dual-layer continuous stretching conductive structure aims to

https://doi.org/10.1021/acsomega.4c06328
ACS Omega 2024, 9, 43743−43755

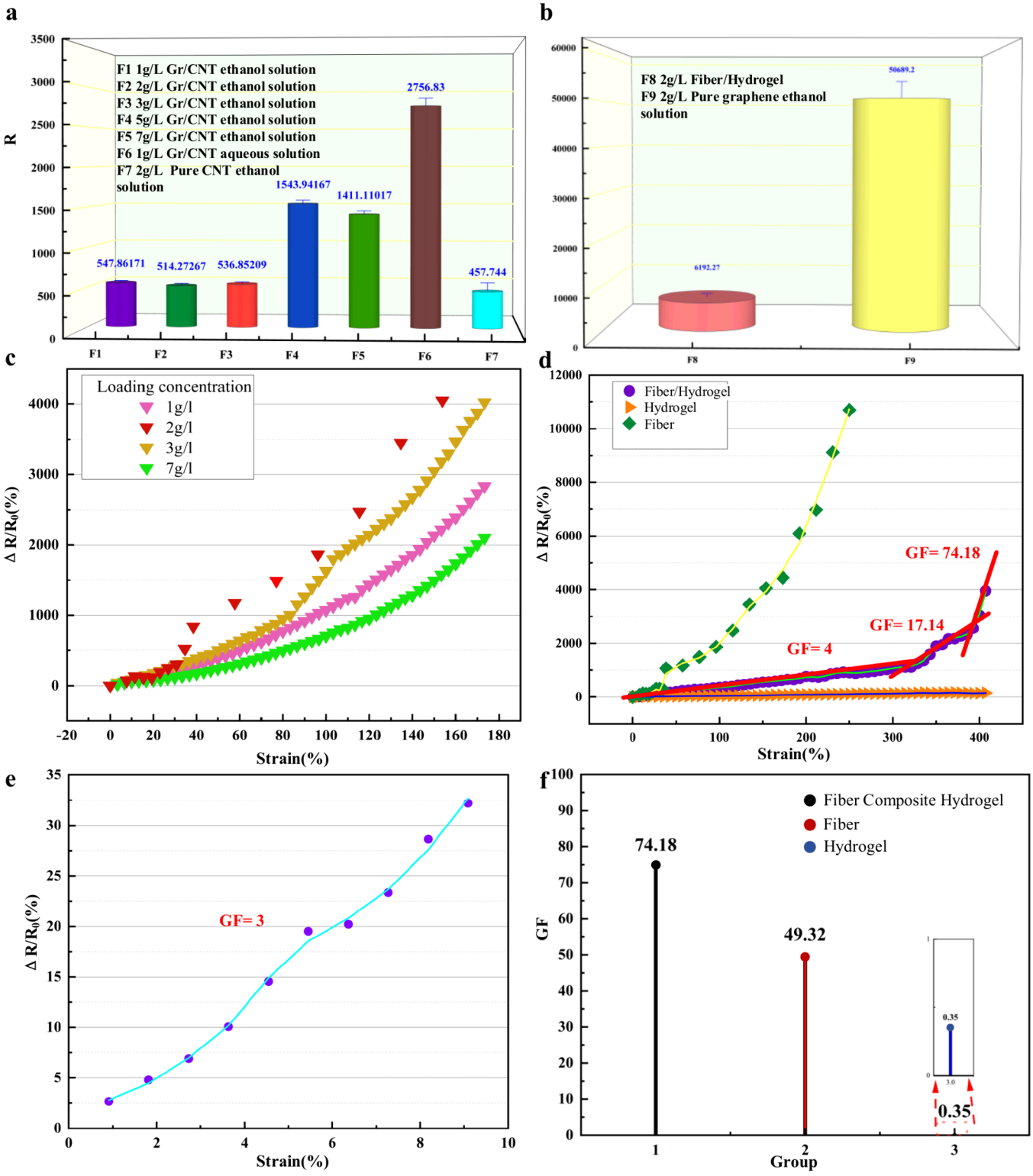

Figure 4. Strain sensor sensing performance. (a, b) Images of the initial resistance of different sensors. (c) Graph depicting the relative change in sensor resistance with strain for different concentrations. (d) Comparative graph showing the relative change in resistance with strain for fiber sensors and hydrogel sensors. (e) Graph illustrating the relative change in sensor resistance with strain. (f) Comparison of sensitivity among different strain sensors.

achieve rapid and accurate high operational range along with high sensitivity. The TPU conductive fiber exhibits high sensitivity but has a limited stretching range (approximately 150%−250%). Meanwhile, the PVA conductive hydrogel has lower sensitivity but a broader stretching range (about 700%). Therefore, the strain sensor designed in this study adopts a parallel resistor configuration, which results in significantly improved sensing performance compared with both individual materials.[44−46] The present study comparatively analyzes the relative changes in sensor resistance signals to demonstrate its

https://doi.org/10.1021/acsomega.4c06328
ACS Omega 2024, 9, 43743−43755

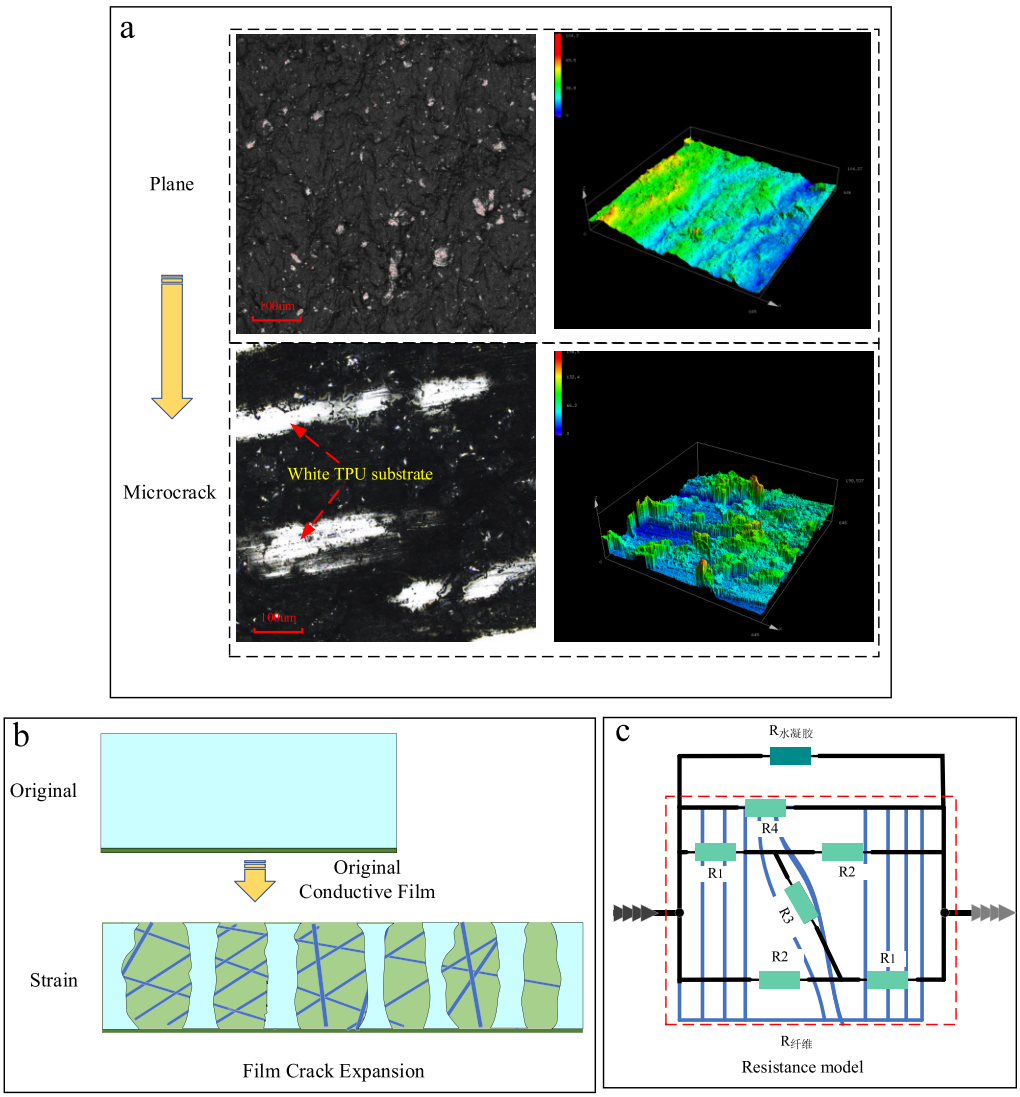

Figure 5. Potential mechanism of TPU/PVA fiber composite hydrogel strain sensors. (a) Morphological images of the sensor on the original and stretched surfaces. (b) Schematic of the sensor morphology. (c) Simple resistance model.

superior electrical performance under various mechanical strain conditions. The loading of Gr/CNT on the fiber membrane imparts robust conductivity and initial resistance to the fiber, as shown in Figure 4a,b. A comparative analysis is conducted to investigate the impact of varying levels of conductive loading and its synergistic correlation on the strain-sensing performance of the sensor. By employing a controlled variable approach to validate the initial resistance of the sensor, different solutions have an impact on fiber loading, as depicted in Figure 4a. Under the same concentration, the initial resistance of Gr/CNT in water solution differs from that in ethanol solution, with the ethanol solution exhibiting a significantly higher initial resistance (547.86 Ω) than the water solution (2756.83 Ω). Similarly, under the condition of a 1:1 ratio of Gr/CNT, different concentrations of Gr/CNT also have an impact on the initial resistance. Among them, the ethanol solution of Gr/CNT with a concentration of 2 g/L exhibits the lowest initial resistance (514.27 Ω). To further explore the issue of initial resistance, the initial resistance of pure Gr is measured to be 50689.20 Ω, while the initial resistance of pure CNT is 457.74Ω. The initial resistance of pure Gr is significantly higher than that of pure CNT. The resistance of composite materials is influenced and balanced by the interplay between two materials, considering the effects of conductivity, changes in current pathways, and interface effects. The overall resistance values lie between the resistances of the two individual materials, in accordance with Ohm's law. The overall resistance increases with the greater content of graphene (Gr). After the optimal concentration is selected, the conductive fibers and hydrogel are combined to prepare the strain sensor. The sensor exhibits a favorable initial resistance, which is positioned between the resistance values of the hydrogel and the conductive fibers, as depicted in Figure 4b.

The conductive nanofibers exhibit excellent sensing performance due to the synergistic effect of Gr/CNT loading. Nanofibers treated with ethanol solutions at concentrations ranging from 1 g/L to 3 g/L exhibit lower initial resistance values. Therefore, this study uses a series of loading variations at concentrations of 1, 2, 3, 7, and so on, to investigate their impact on the behavior of the strain sensor. As shown in Figure 4c, sensitivity is represented as GF, which is defined as the ratio of resistance change to strain.

$$GF = (R - R_0)/\varepsilon R_0 \quad (1)$$

https://doi.org/10.1021/acsomega.4c06328
ACS Omega 2024, 9, 43743−43755

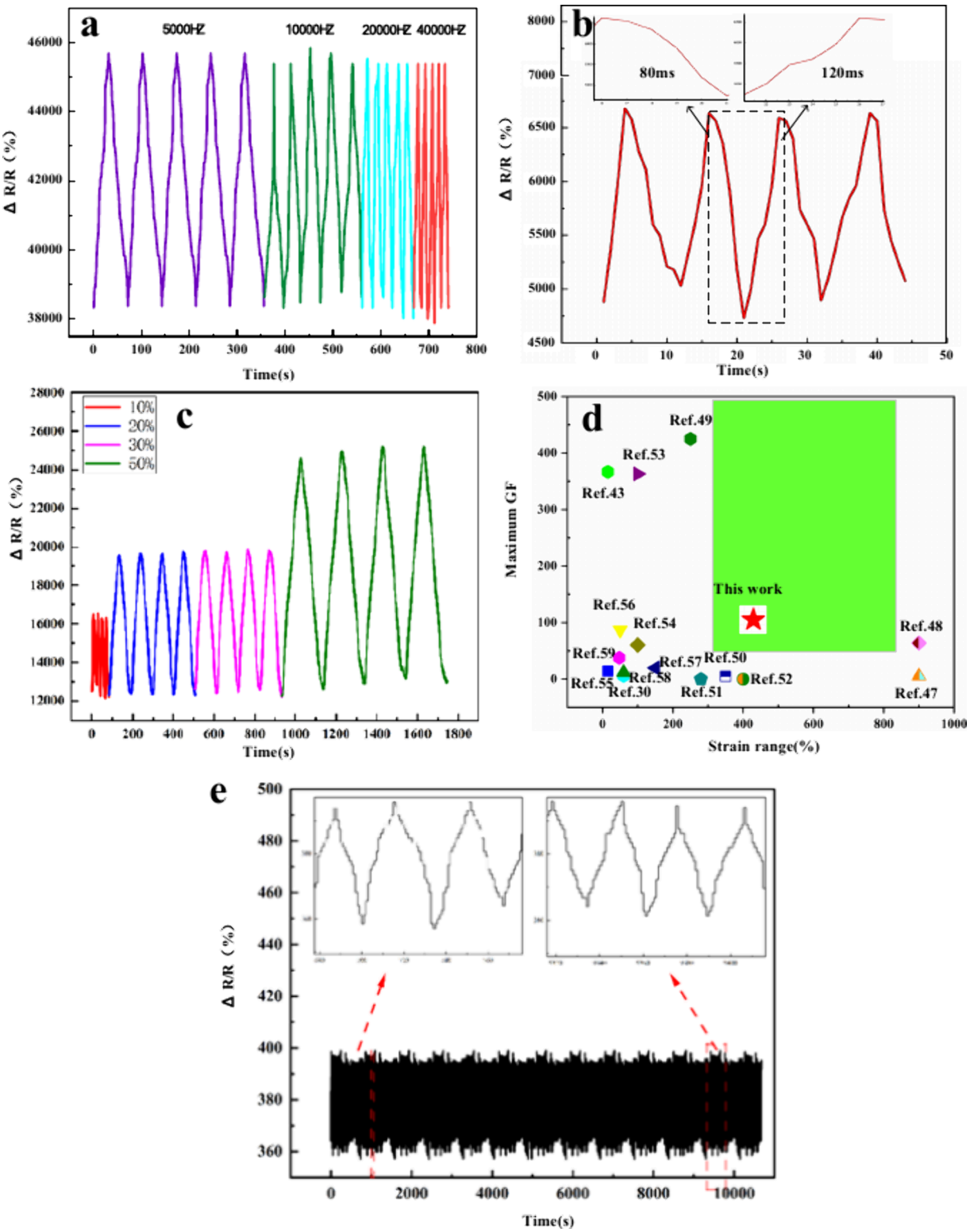

Figure 6. Electromechanical performance of the strain sensor made of TPU fiber and PVA hydrogel. (a) Relative resistance change of the strain sensor at different strain rates. (b) Response time of the strain sensor when subjected to a 3% strain at a strain rate of 20,000 Hz. (c) Relative resistance change of the strain sensor at different strains. (d) Comparison of sensitivity and operating range with previously reported stretchable strain sensors.[30,45,48−60] (e) Strain response behavior of the strain sensor during 800 cycles at a 50% strain.

$$\varepsilon = (L - L_0)/L_0 \quad (2)$$

Here, R, R_0, L, L_0, and ε represent real-time resistance, initial resistance, elongation length, initial length, and strain, respectively.[1,47] The graph clearly illustrates that nanofibers treated with ethanol solution at a concentration of 7 g/L exhibit the lowest sensitivity, while those treated with a concentration of 2 g/L show the highest sensitivity. Therefore, this study uses nanofibers treated with a 2 g/L ethanol solution to prepare the strain sensor. As shown in Figure 4d,e, the

https://doi.org/10.1021/acsomega.4c06328
ACS Omega 2024, 9, 43743−43755

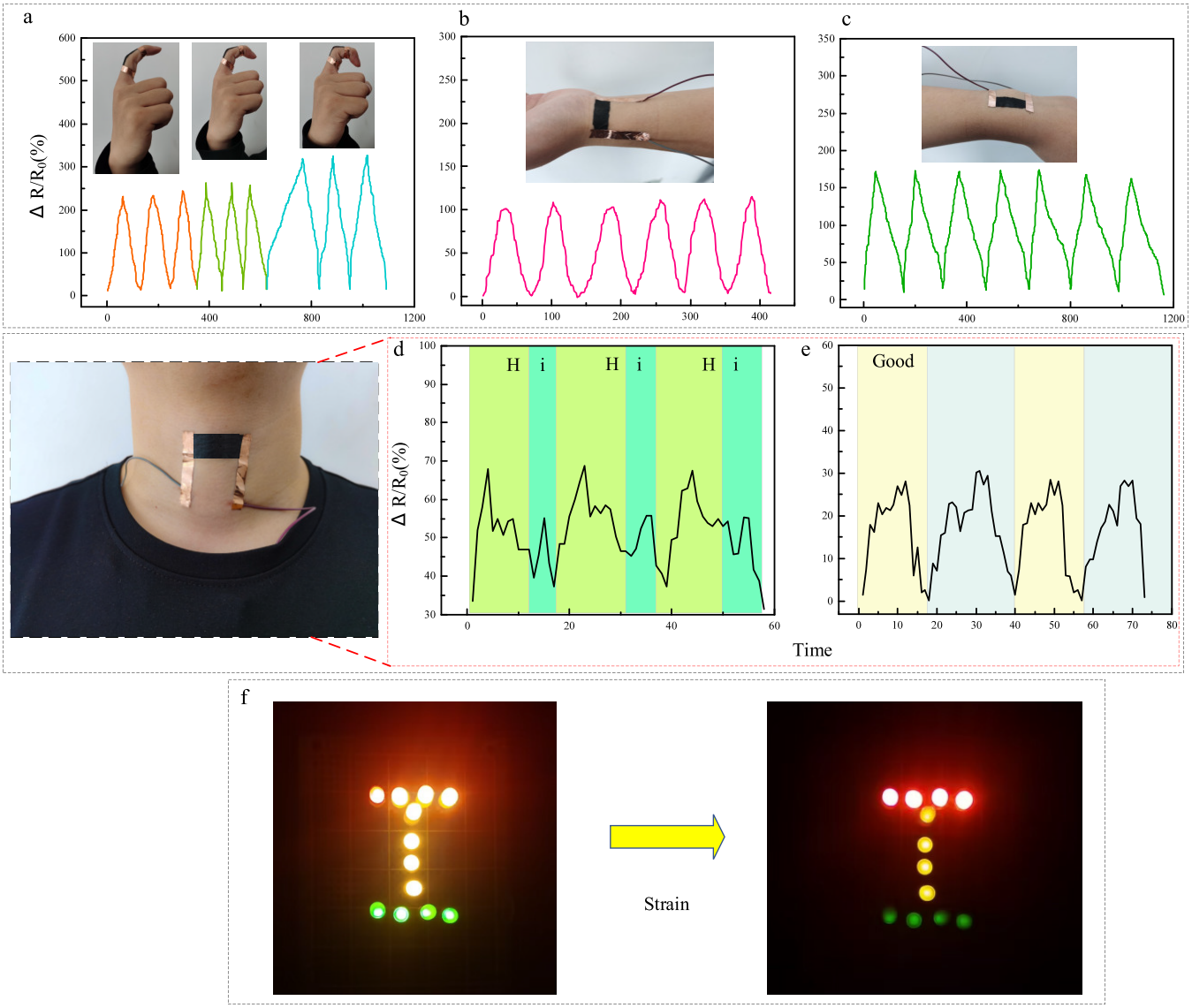

Figure 7. Practical applications of sensors. (a) Finger movements at different angles, (b) pulsatile fluctuations, (c) wrist motions, (d, e) resistance response behaviors to various vocalization methods, and (f) changes in the brightness of a light bulb during stretching movements.

resistance of the sensor during the stretching process exhibits an increasing trend. This improvement is primarily attributed to changes in the conductive network after stretching, which leads to a rise in resistance. The conductive fiber strain sensor, while exhibiting high sensitivity (GF 49.32), has a limited stretching range. Meanwhile, the hydrogel demonstrates a broad stretching range but lower sensitivity (GF 0.35). The dual-layer continuous strain sensor made from a composite hydrogel containing conductive fibers exhibits a sensitivity of 4 within the strain range of 10%−300%, a sensitivity of 17.14 within the range of 300%−385%, and a remarkably high sensitivity of 74.18 within the range of 385%−400%. Moreover, the sensor maintains good sensitivity (GF 3) even in detecting minimal deformations (0.6%). Notably, the sensor demonstrates a linear response within the strain range of 0%−330%.

During the stretching process, the resistance of the sensor undergoes continuous changes. Therefore, a basic exploration of the underlying mechanism of strain sensors is conducted. In the stretching process at lower strain levels, the conductive material of Gr/CNT adhered to the surface of TPU fibers in the strain sensor can be considered a thin film. The fracture of the thin film results in gaps and islands. As the strain increases, the number and width of these gaps and islands rise. This explanation attributes the increase in resistance to the fracture of the thin film network, which realizes higher sensitivity. At higher strain levels, the Gr/CNT conductive network undergoes complete fracture, which consequently limits the operational range of the sensor. During the macro-scale stretching process, white lines and microcracks appear on the black TPU fibers (Figure 5a,b). In the case of the double-layer continuous strain sensor made from a composite hydrogel containing conductive fibers at low strains, the conductive fibers play a more significant role than the hydrogel. Therefore, the sensitivity is only slightly lower than that of the conductive fibers alone. However, at high strains, the double-layer continuous strain sensor ensures rapid healing of the Gr/CNT conductive network after fracture due to the highly viscous nature of the hydrogel. Moreover, when the Gr/CNT conductive network undergoes complete fracture, the hydrogel

https://doi.org/10.1021/acsomega.4c06328
ACS Omega 2024, 9, 43743−43755

Table 1. Material Information in the Experiment

Name	Company
Polyvinyl alcohol, PVA	Sinopharm Chemical Reagent Corporation
Thermoplastic polyurethanes, TPU 75A. molecular mass 90K	Taiwan Risheng Corporation
N,N-Dimethylformamide, DMF	Shanghai Sinopharm Group Chemical Reagent Company
Tetrahydrofuran, THF	Sarn Chemical Technology (Shanghai) Corporation
Carbon nanofoam, CNT	Shanghai Chaowei Nano Technology Co.
Graphene, Gr	Suzhou Carbonfund Graphene Technology Co.
Sodium dodecyl sulfonate	Suzhou Carbonfund Graphene Technology Co.
Ethylene glycol, EG	Sinopharm Chemical Reagent Corporation
Anhydrous ethanol	Shanghai Sinopharm Group Chemical Reagent Company
Borax	Shanghai McLean Biochemical Technology Co.
Sodium periodate	Sarn Chemical Technology (Shanghai) Co.
Glutaraldehyde	Shanghai Marel Chemical Technology Co.

takes on a dominant role. In addition, high sensitivity is ensured at large strains due to the adhesion of Gr/CNT on the surface of the conductive hydrogel. Furthermore, the presence of CNTs and graphene forms an effective conductive network. The opening and closing of the conductive pathways in the network result in changes in resistance. These changes impart sensing capabilities to the sensor. Under the synergistic effect of the two materials, the performance of the sensor is further enhanced. The graphene within the sensor, with its two-dimensional layered structure, extends across a large planar area, which provides numerous active sites. Meanwhile, the CNTs, with their one-dimensional hollow cylindrical structure and high aspect ratio, contribute to the formation of a three-dimensional network when combined with graphene. This network not only exhibits high electrical conductivity but also offers additional active sites within the structure, which increase the sensitivity of the sensor. The macroscopic total resistance of the resistive double-layer continuous strain sensor made from a composite hydrogel containing conductive fibers can be regarded as the sum of parallel resistances, as illustrated in Figure 5c.

$$R = (R_{\text{fibroid}} \times R_{\text{hydrogel}})/(R_{\text{fibroid}} + R_{\text{hydrogel}}) \quad (3)$$

The simple resistance model for fiber membranes is expressed as eq 4.

$$R = \frac{R_1R_3 + 2R_1R_2 + R_2R_3}{R_1 + 2R_3 + R_2} \quad (4)$$

R_1 represents Gr/CNT islands, R_2 corresponds to cracked Gr/CNT layers, and R_3 denotes the bridge resistance between adjacent islands.[44,48]

The behavior of the sensor under different strain amplitudes in cyclic strain sensing is investigated. As shown in Figure 6a, the can produce stable and reproducible sensing signals across a wide range of strains. The upper and lower limits of detection are 0.6% and 400%, respectively. The strain response behavior under different tensile rates is also explored, as depicted in Figure 6c. The strain sensing behavior exhibited by the sensor appears to be independent of the strain rate. A cyclic stretching test at a 3% strain and 20,000 Hz is conducted to validate the rapid detection capability of the sensor. As shown Figure 6b, the response time is 80 ms with a recovery time of 120 ms. This combination forms the foundational assurance for the responsiveness of the sensor even during detection of various human movements. Furthermore, this study conducts tests on the strain response behavior of the sensor during 800 cycles at a 50% strain to verify its long-term durability, as illustrated in Figure 6e. The strain response demonstrates recoverability and reproducibility, with the response peak maintaining a good balance throughout the testing process. This performance indicates excellent durability of the sensor. High-performance wearable flexible strain sensors can rapidly and accurately identify and detect full-body movements. This capability necessitates that flexible sensors possess a strain range greater than 55% and a sensitivity greater than 2. The maximum sensitivity and detection range of the multilayer conductive nanofiber sensor are compared with sensors from existing literature, as depicted in Figure 6d.

4. APPLICATIONS

The prepared flexible strain sensors can detect various human movements due to their excellent sensitivity and other characteristics, and this capability is a significant advantage in wearable devices. The responsiveness of the sensor to pulse beating is demonstrated through subtle human movements, as illustrated in Figure 7b. Figure 7d,e depict the resistance response behavior to throat sound production, which shows distinct signals for uttering “Hi” and “Good.” This result indicates the high sensitivity and accuracy of the sensor in detecting subtle signals. In addition, the sensor can detect larger human movements. Figure 7a shows the response behavior of the sensor to finger movements at different temperatures (30 °C, 60 °C, and 90 °C), while Figure 7c illustrates the response to wrist movements. The wide detection range of the sensor is evident, which maintains clear and reproducible signals. In terms of electronic applications, as shown in Figure 7f, the brightness of the light bulb decreases during the stretching process.

5. CONCLUSIONS

In addressing the challenges of a wide detection range, high sensitivity, rapid response, and low detection of strain sensors, this study proposes a dual-layer continuous conductive structure integrating a strain sensor made from a composite hydrogel containing conductive fibers of TPU and PVA. Sensitivity testing, stretching range detection, and a series of experimental studies on response time are conducted. The following conclusions are drawn:

(1) In the flexible strain sensor, a dual-layer conductive load is formed, which extends the working range from 250% to 400%. This method effectively utilizes the ability of the hydrogel to mitigate the tendency of the Gr/CNT conductive network to fracture. It is a simple solution to

https://doi.org/10.1021/acsomega.4c06328
ACS Omega 2024, 9, 43743−43755

the challenges posed by the need for prestraining in fiber sensors to achieve a high working range.

(2) The flexible sensor achieves a sensitivity of 74.18, which significantly outperforms those of the fiber sensor (GF 49.32) and the hydrogel sensor (GF 0.35). The sensor combines the advantages of fiber and hydrogel sensors, which makes it suitable for a wider range of applications.

(3) By addressing the common challenges of detecting minor deformations and achieving rapid response in strain sensors, this study successfully increases the detection range to 0.6%, with response and recovery times improved to 80 and 120 ms, respectively. In addition, the sensor demonstrates excellent performance after 800 durability cycles.

6. MATERIALS

The material information used in the experiment is shown in Table 1.

■ ASSOCIATED CONTENT

Data Availability Statement

No data was used for the research described in the article.

■ AUTHOR INFORMATION

Corresponding Author

Min Yang − *Key Lab of Industrial Fluid Energy Conservation and Pollution Control, Ministry of Education, Qingdao University of Technology, Qingdao 266033, China; College of Physics, Qingdao University, Qingdao 266071, China;* orcid.org/0000-0003-4900-2149; Email: 18266487809@163.com

Authors

Ming Kong − *Key Lab of Industrial Fluid Energy Conservation and Pollution Control, Ministry of Education, Qingdao University of Technology, Qingdao 266033, China*

Ruiyu Zhou − *Key Lab of Industrial Fluid Energy Conservation and Pollution Control, Ministry of Education, Qingdao University of Technology, Qingdao 266033, China*

Jun Zhang − *College of Physics, Qingdao University, Qingdao 266071, China*

Xiao Ma − *Key Lab of Industrial Fluid Energy Conservation and Pollution Control, Ministry of Education, Qingdao University of Technology, Qingdao 266033, China*

Teng Gao − *Key Lab of Industrial Fluid Energy Conservation and Pollution Control, Ministry of Education, Qingdao University of Technology, Qingdao 266033, China*

Yanbin Zhang − *Key Lab of Industrial Fluid Energy Conservation and Pollution Control, Ministry of Education, Qingdao University of Technology, Qingdao 266033, China*

Benkai Li − *Key Lab of Industrial Fluid Energy Conservation and Pollution Control, Ministry of Education, Qingdao University of Technology, Qingdao 266033, China*

Mingzheng Liu − *Key Lab of Industrial Fluid Energy Conservation and Pollution Control, Ministry of Education, Qingdao University of Technology, Qingdao 266033, China*

Xin Cui − *Key Lab of Industrial Fluid Energy Conservation and Pollution Control, Ministry of Education, Qingdao University of Technology, Qingdao 266033, China*

Yunze Long − *College of Physics, Qingdao University, Qingdao 266071, China*

Changhe Li − *Key Lab of Industrial Fluid Energy Conservation and Pollution Control, Ministry of Education, Qingdao University of Technology, Qingdao 266033, China*

Complete contact information is available at: https://pubs.acs.org/10.1021/acsomega.4c06328

Notes

The authors declare no competing financial interest.

■ ACKNOWLEDGMENTS

This study was financially supported by the National Natural Science Foundation of China (Grant Nos. 52205481, 52375447), Support plan for Outstanding Youth Innovation Team in Universities of Shandong Province (2023KJ114), Qingdao Science and Technology Planning Park Cultivation Plan (23-1-5-yqpy-17-qy).

■ REFERENCES

(1) Xiao, X.; Yuan, L.; Zhong, J.; Ding, T.; Liu, Y.; Cai, Z.; Rong, Y.; Han, H.; Zhou, J.; Wang, Z. L. High-strain sensors based on ZnO nanowire/polystyrene hybridized flexible films. *Adv. Mater.* **2011**, *23*, 5440−5444.

(2) Ma, Y.; Cheng, Y.; Wang, J.; Fu, S.; Zhou, M.; Yang, Y.; Li, B.; Zhang, X.; Nan, C. W. Flexible and highly-sensitive pressure sensor based on controllably oxidized MXene. *InfoMat* **2022**, *4*, No. e12328.

(3) Li, H.; Hu, Z.; Xia, Q.; Zhang, H.; Li, Z.; Wang, H.; Li, X.; Zuo, F.; Zhang, F.; Wang, X.; Ye, W.; Li, Q.; Long, Y.; Li, Q.; Yan, S.; Liu, X.; Zhang, X.; Yu, G.; Miao, G. X. Operando Magnetometry Probing the Charge Storage Mechanism of CoO Lithium-Ion Batteries. *Adv. Mater.* **2021**, *33*, No. e2006629.

(4) Sun, H.; Bu, Y.; Liu, H.; Wang, J.; Yang, W.; Li, Q.; Guo, Z.; Liu, C.; Shen, C. Superhydrophobic conductive rubber band with synergistic dual conductive layer for wide-range sensitive strain sensor. *Sci. Bull. (Beijing).* **2022**, *67*, 1669−1678.

(5) Liao, X.; Song, W.; Zhang, X.; Jin, H.; Liu, S.; Wang, Y.; Thean, A. V. Y.; Zheng, Y. An Artificial Peripheral Neural System Based on Highly Stretchable and Integrated Multifunctional Sensors. *Adv. Funct. Mater.* **2021**, *31*, No. 2101107.

(6) Kong, M.; Yang, M.; Li, R.; Long, Y.-Z.; Zhang, J.; Huang, X.; Cui, X.; Zhang, Y.; Said, Z.; Li, C. Graphene-based flexible wearable sensors: mechanisms, challenges, and future directions. *Int. J. Adv. Manuf Technol.* **2024**, *131*, 3205.

(7) Puneetha, P.; Mallem, S. P. R.; Park, S. C.; Kim, S.; Heo, D. H.; Kim, C. M.; Shim, J.; An, S. J.; Lee, D.-Y.; Park, K.-I. Ultra-flexible graphene/nylon/PDMS coaxial fiber-shaped multifunctional sensor. *Nano Res.* **2023**, *16*, 5541−5547.

(8) Zhang, H.; Zhang, J.; Zhang, Y.; Ye, X.; Li, Y.; Wang, P. Application of flexible pressure sensor based on AgNWs in human motion detection. *International Journal of Clothing Science and Technology.* **2023**, *35*, 312−319.

(9) Niu, Z.; Cheng, W.; Cao, M.; Wang, D.; Wang, Q.; Han, J.; Long, Y.; Han, G. Recent advances in cellulose-based flexible triboelectric nanogenerators. *Nano Energy* **2021**, *87*, No. 106175.

(10) Shen, T.; Liu, S.; Yue, X.; Wang, Z.; Liu, H.; Yin, R.; Liu, C.; Shen, C. High-performance fibrous strain sensor with synergistic sensing layer for human motion recognition and robot control. *Adv. Compos. Hybrid Mater.* **2023**, *6*, 127.

(11) Wang, J.; Liu, H.; Yue, X.; Zhang, D.; Yin, R.; Sun, H.; Liu, C.; Shen, C. Large-scale fabrication of conductive yarn with synergistic conductive coating for high-efficient strain sensing and photothermal conversion. *Materials Today Nano.* **2023**, *24*, No. 100427.

(12) Chen, Z.; Lin, W.; Zhang, C.; Xu, Y.; Wei, C.; Hu, H.; Liao, X.; Chen, Z. Multifunctional and Reconfigurable Electronic Fabrics Assisted by Artificial Intelligence for Human Augmentation. *Adv. Fiber Mater.* **2024**, *6*, 229−242.

(13) Luo, Y.; Abidian, M. R.; Ahn, J.-H.; Akinwande, D.; Andrews, A. M.; Antonietti, M.; et al. Technology Roadmap for Flexible Sensors. *ACS Nano* **2023**, *17*, 5211−5295.
(14) Liu, H.; Zhang, H.; Han, W.; Lin, H.; Li, R.; Zhu, J.; Huang, W. 3D Printed Flexible Strain Sensors: From Printing to Devices and Signals. *Adv. Mater.* **2021**, *33*, No. e2004782.
(15) Zhang, J.; Wang, Y.; Wei, Q.; Wang, Y.; Lei, M.; Li, M.; Li, D.; Zhang, L.; Wu, Y. Self-Healing Mechanism and Conductivity of the Hydrogel Flexible Sensors: A Review. *Gels.* **2021**, *7*, 216.
(16) Shen, Z.; Liu, F.; Huang, S.; Wang, H.; Yang, C.; Hang, T.; Tao, J.; Xia, W.; Xie, X. Progress of flexible strain sensors for physiological signal monitoring. *Biosens Bioelectron.* **2022**, *211*, No. 114298.
(17) Yang, M.; Li, C.; Luo, L.; Li, R.; Long, Y. Predictive model of convective heat transfer coefficient in bone micro-grinding using nanofluid aerosol cooling. *Int. Commun. Heat Mass Transfer.* **2021**, *125*, No. 105317.
(18) Yang, W.; Liu, S.; Wang, Z.; Liu, H.; Pan, C.; Liu, C.; Shen, C. Bioinspired composite fiber aerogel pressure sensor for machine-learning-assisted human activity and gesture recognition. *Nano Energy.* **2024**, *127*, No. 109799.
(19) Liao, X.; Wang, W.; Wang, L.; Jin, H.; Shu, L.; Xu, X.; Zheng, Y. A highly stretchable and deformation-insensitive bionic electronic exteroceptive neural sensor for human-machine interfaces. *Nano Energy.* **2021**, *80*, No. 105548.
(20) Shen, Y.; Yang, W.; Hu, F.; Zheng, X.; Zheng, Y.; Liu, H.; Algadi, H.; Chen, K. Ultrasensitive wearable strain sensor for promising application in cardiac rehabilitation. *Adv. Compos. Hybrid Mater.* **2023**, *6*, 21.
(21) Zheng, H.; Wang, H.; Yi, K.; Lin, J.; Chen, A.; Chen, L.; Zou, Z.; Liu, M.; Ji, Y.; Dong, L.; Lin, Z. Wearable LIG Flexible Stress Sensor Based on Spider Web Bionic Structure. *Coatings* **2023**, *13*, 155.
(22) Wang, W.; Ma, Y.; Wang, T.; Ding, K.; Zhao, W.; Jiao, L.; Shu, D.; Li, C.; Hua, F.; Jiang, H.; Tong, S.; Yang, S.; Ni, Y.; Cheng, B. Double-Layered Conductive Network Design of Flexible Strain Sensors for High Sensitivity and Wide Working Range. *ACS Appl. Mater. Interfaces.* **2022**, *14*, 36611−36621.
(23) Yang, M.; Cheng, Y.; Yue, Y.; Chen, Y.; Gao, H.; Li, L.; Cai, B.; Liu, W.; Wang, Z.; Guo, H.; Liu, N.; Gao, Y. High-Performance Flexible Pressure Sensor with a Self-Healing Function for Tactile Feedback. *Adv. Sci. (Weinh).* **2022**, *9*, No. e2200507.
(24) Shen, Z.; Zhang, Z.; Zhang, N.; Li, J.; Zhou, P.; Hu, F.; Rong, Y.; Lu, B.; Gu, G. High-Stretchability, Ultralow-Hysteresis ConductingPolymer Hydrogel Strain Sensors for Soft Machines. *Adv. Mater.* **2022**, *34*, No. e2203650.
(25) He, Z.; Liu, J.; Fan, X.; Song, B.; Gu, H. Tara Tannin-Cross-Linked, Underwater-Adhesive, Super Self-Healing, and Recyclable Gelatin-Based Conductive Hydrogel as a Strain Sensor. *Ind. Eng. Chem. Res.* **2022**, *61*, 17915−17929.
(26) Xu, L.; Huang, Z.; Deng, Z.; Du, Z.; Sun, T. L.; Guo, Z. H.; Yue, K. A Transparent, Highly Stretchable, Solvent-Resistant, Recyclable Multifunctional Ionogel with Underwater Self-Healing and Adhesion for Reliable Strain Sensors. *Adv. Mater.* **2021**, *33*, No. e2105306.
(27) Ke, T.; Zhao, L.; Fan, X.; Gu, H. Rapid self-healing, self-adhesive, anti-freezing, moisturizing, antibacterial and multi-stimuli-responsive PVA/starch/tea polyphenol-based composite conductive organohydrogel as flexible strain sensor. *J. Mater. Sci. Technol.* **2023**, *135*, 199−212.
(28) Yang, Y.; Wang, H.; Hou, Y.; Nan, S.; Di, Y.; Dai, Y.; Li, F.; Zhang, J. MWCNTs/PDMS composite enabled printed flexible omnidirectional strain sensors for wearable electronics. *Compos. Sci. Technol.* **2022**, *226*, No. 109518.
(29) Gong, H.; Wang, Z.; Cheng, Z.; Chen, L.; Pan, H.; Zhang, D.; Hu, T.; Tyasi, T. L. Flexible Strain Sensor Based on 3D Electrospun Carbonized Sponge. *Comput., Mater. Continua* **2022**, *73*, 4971−4980.
(30) Huang, L.; Wang, H.; Wu, P.; Huang, W.; Gao, W.; Fang, F.; Cai, N.; Chen, R.; Zhu, Z. Wearable Flexible Strain Sensor Based on Three-Dimensional Wavy Laser-Induced Graphene and Silicone Rubber. *Sensors (Basel).* **2020**, *20*, 4266.
(31) Chen, B.; Liu, Y.; Wang, G.; Cheng, X.; Liu, G.; Qiu, J.; Lv, K. Low-Cost Flexible Strain Sensor Based on Thick CVD Graphene. *Nano* **2018**, *13*, No. 1850126.
(32) Zhang, H.; Han, W.; Xu, K.; Zhang, Y.; Lu, Y.; Nie, Z.; Du, Y.; Zhu, J.; Huang, W. Metallic Sandwiched-Aerogel Hybrids Enabling Flexible and Stretchable Intelligent Sensor. *Nano Lett.* **2020**, *20*, 3449−3458.
(33) Feng, Y.; Liu, H.; Zhu, W.; Guan, L.; Yang, X.; Zvyagin, A. V.; Zhao, Y.; Shen, C.; Yang, B.; Lin, Q. Muscle-Inspired MXene Conductive Hydrogels with Anisotropy and Low-Temperature Tolerance for Wearable Flexible Sensors and Arrays. *Adv. Funct. Mater.* **2021**, *31*, No. 2105264.
(34) Yue, X.; Fang, C.; Yao, Q.; Liu, C.; Shen, C.; Liu, H. Tunable porous fiber-shaped strain sensor with synergistic conductive network for human motion recognition and tactile sensing. *Chemical Engineering Journal.* **2024**, *491*, No. 151853.
(35) Tian, Y.; Huang, M.; Wang, Y.; Zheng, Y.; Yin, R.; Liu, H.; Liu, C.; Shen, C. Ultra-stretchable, sensitive and breathable electronic skin based on TPU electrospinning fibrous membrane with microcrack structure for human motion monitoring and self-powered application. *Chemical Engineering Journal.* **2024**, *480*, No. 147899.
(36) Fang, F.; Wang, H.; Wang, H.; Huang, W. M.; Chen, Y.; Cai, N.; Chen, X.; Chen, X. Stimulus-Responsive Shrinkage in Electrospun Membranes: Fundamentals and Control. *Micromachines* **2021**, *12*, 920.
(37) Zhang, H. Flexible textile-based strain sensor induced by contacts. *Meas. Sci. Technol.* **2015**, *26*, No. 105102.
(38) Zhang, Y.; Li, C.; Zhou, B.; He, H.; Zhou, Y.; Jiang, L.; Zhou, F. L.; Chen, S. A flexible strain sensor based on conductive TPU/CNTs-Gr composites. *J. Appl. Polym. Sci.* **2022**, *139*, No. e52475.
(39) Yu, X.; Wu, Z.; Weng, L.; Jiang, D.; Algadi, H.; Qin, Z.; Guo, Z.; Xu, B. B. Flexible Strain Sensor Enabled by Carbon Nanotubes-Decorated Electrospun TPU Membrane for Human Motion Monitoring. *Adv. Mater. Interfaces* **2023**, *10*, No. 2202292.
(40) Xiang, D.; Chen, X.; Li, J.; Wu, Y.; Zhao, C.; Li, H.; Li, Z.; Wang, L.; Wang, P.; Li, Y.; Wang, J. Flexible strain sensors with high sensitivity and large working range prepared from biaxially stretched carbon nanotubes/polyolefin elastomer nanocomposites. *J. Appl. Polym. Sci.* **2023**, *140*, No. e53371.
(41) Wang, Y.; Yang, R.; Shi, Z.; Zhang, L.; Shi, D.; Wang, E.; Zhang, G. Super-elastic graphene ripples for flexible strain sensors. *ACS Nano* **2011**, *5*, 3645−3650.
(42) Chen, C.; Chu, F.; Zhang, Y.; Ma, M.; Sun, R.; Jia, P.; Sun, J. Fabricating Flexible Strain Sensor with Direct Writing Graphene/Carbon Nanotube Aerogel. *ACS Appl. Electron. Mater.* **2023**, *5*, 1429−1436.
(43) Chen, Y.; Fu, X.; Kang, S.; Wang, L.; Lu, W. Strategy of Fabricating Flexible Strain Sensor via Layer-by-Layer Assembly of Conductive Hydrogels. *ACS Appl. Electron. Mater.* **2021**, *3*, 3889−3897.
(44) Jiang, Y.; Liang, F.; Li, H. Y.; Li, X.; Fan, Y. J.; Cao, J. W.; Yin, Y. M.; Wang, Y.; Wang, Z. L.; Zhu, G. A Flexible and Ultra-Highly Sensitive Tactile Sensor through a Parallel Circuit by a Magnetic Aligned Conductive Composite. *ACS Nano* **2022**, *16*, 746−754.
(45) Zhao, D.; Zhang, Q.; Liu, Y.; Zhang, Y.; Guo, X.; Yuan, Z.; Zhang, W.; Zhang, R.; Lian, J. W.; Sang, S. Highly sensitive and flexible strain sensor based on AuNPs/CNTs synergic conductive network. *Appl. Nanosci.* **2019**, *9*, 1469−1478.
(46) Cheng, W.; Wang, J.; Ma, Z.; Yan, K.; Wang, Y.; Wang, H.; Li, S.; Li, Y.; Pan, L.; Shi, Y. Flexible Pressure Sensor With High Sensitivity and Low Hysteresis Based on a Hierarchically Micro-structured Electrode. *IEEE Electron Device Lett.* **2018**, *39*, 288−291.
(47) Wang, M.; Mu, L.; Zhang, H.; Ma, S.; Liang, Y.; Ren, L. Flexible strain sensor with ridge-like microstructures for wearable applications. *Polym. Adv. Technol.* **2022**, *33*, 96−103.
(48) Yamada, T.; Hayamizu, Y.; Yamamoto, Y.; Yomogida, Y.; Izadi-Najafabadi, A.; Futaba, D. N.; Hata, K. A stretchable carbon nanotube

https://doi.org/10.1021/acsomega.4c06328
ACS Omega 2024, 9, 43743−43755

strain sensor for human-motion detection. *Nat. Nanotechnol.* **2011**, *6*, 296−301.
(49) Ren, M.; Zhou, Y.; Wang, Y.; Zheng, G.; Dai, K.; Liu, C.; Shen, C. Highly stretchable and durable strain sensor based on carbon nanotubes decorated thermoplastic polyurethane fibrous network with aligned wave-like structure. *Chemical Engineering Journal.* **2019**, *360*, 762−777.
(50) Ryu, S.; Lee, P.; Chou, J. B.; Xu, R.; Zhao, R.; Hart, A. J.; Kim, S. G. Extremely Elastic Wearable Carbon Nanotube Fiber Strain Sensor for Monitoring of Human Motion. *ACS Nano* **2015**, *9*, 5929−5936.
(51) Zhou, J.; Xu, X.; Xin, Y.; Lubineau, G. Coaxial Thermoplastic Elastomer-Wrapped Carbon Nanotube Fibers for Deformable and Wearable Strain Sensors. *Adv. Funct. Mater.* **2018**, *28*, 1705591.
(52) Cai, G.; Hao, B.; Luo, L.; Deng, Z.; Zhang, R.; Ran, J.; Tang, X.; Cheng, D.; Bi, S.; Wang, X.; Dai, K. Highly Stretchable Sheath-Core Yarns for Multifunctional Wearable Electronics. *ACS Appl. Mater. Interfaces.* **2020**, *12*, 29717−29727.
(53) Yu, Y.; Luo, Y.; Guo, A.; Yan, L.; Wu, Y.; Jiang, K.; Li, Q.; Fan, S.; Wang, J. Flexible and transparent strain sensors based on super-aligned carbon nanotube films. *Nanoscale.* **2017**, *9*, 6716−6723.
(54) Wang, H.; Zhou, R.; Li, D.; Zhang, L.; Ren, G.; Wang, L.; Liu, J.; Wang, D.; Tang, Z.; Lu, G.; Sun, G.; Yu, H. D.; Huang, W. High-Performance Foam-Shaped Strain Sensor Based on Carbon Nanotubes and Ti_3C_2Tx MXene for the Monitoring of Human Activities. *ACS Nano* **2021**, *15*, 9690−9700.
(55) Ding, Y. R.; Xue, C. H.; Guo, X. J.; Wang, X.; Jia, S. T.; An, Q. F. Flexible Superamphiphobic Film with a 3D Conductive Network for Wearable Strain Sensors in Humid Conditions. *ACS Appl. Electron. Mater.* **2022**, *4*, 345−355.
(56) Zhang, M.; Wang, C.; Wang, Q.; Jian, M.; Zhang, Y. Sheath-Core Graphite/Silk Fiber Made by Dry-Meyer-Rod-Coating for Wearable Strain Sensors. *ACS Appl. Mater. Interfaces.* **2016**, *8*, 20894−20899.
(57) Li, X.; Hua, T.; Xu, B. Electromechanical properties of a yarn strain sensor with graphene-sheath/polyurethane-core. *Carbon.* **2017**, *118*, 686−698.
(58) Souri, H.; Bhattacharyya, D. Wearable strain sensors based on electrically conductive natural fiber yarns. *Mater. Des.* **2018**, *154*, 217−227.
(59) Chun, S.; Son, W.; Park, W. A Stretchable Graphene Thin-Film Sensor for Detecting All of Lateral and Vertical Strains. *J. Nanosci. Nanotechnol.* **2019**, *19*, 1585−1591.
(60) Zhang, L.; Li, H.; Lai, X.; Gao, T.; Zeng, X. Three-Dimensional Binary-Conductive-Network Silver Nanowires@Thiolated Graphene Foam-Based Room-Temperature Self-Healable Strain Sensor for Human Motion Detection. *ACS Appl. Mater. Interfaces.* **2020**, *12*, 44360−44370.

https://doi.org/10.1021/acsomega.4c06328
ACS Omega 2024, 9, 43743−43755